

Methods for measuring noise, purity changes, and entanglement entropy in quantum devices and systems

Raam Uzdin

December 2, 2021

Abstract

We present methods for evaluating the rate of change in quantities during quantum evolution due to coupling to the environment (dissipation hereafter). The protocol is based on repeating a given quantum circuit (or quantum operation) twice, thrice, and so on, and measuring an expectation value after each number of repetitions. We start by applying this method for measuring the rate of purity changes in quantum circuits. This provides direct information on the quality of the circuit. Furthermore, the presented scheme enables to distill the dissipative contribution in the changes of quantities such as energies and coherence. In particular, this can be applied to the local Hamiltonians of specific qubits. Thus, our approach can be used to locate “hotspots” where the dissipation takes place. A variant of this method can be used to measure the entanglement buildup in quantum circuits. These methods are scalable as they involve only a few observables which are relatively easy to measure in NISQ devices.

1 Introduction

The premise of quantum technology and quantum computing is to provide a dramatic improvement compared to classical devices. In particular, quantum computers and simulators should help solve with finite resources (time, memory, energy, etc.) problems that would otherwise require unrealistic resources. The complicated nature of quantum evolution makes error detection and diagnostics very challenging. If the output cannot be computed by some other means, it is difficult to crosscheck and rule out the possibility that the device is either defective to begin with, or it had malfunctioned during its operation. This is especially true in the several dozen qubits NISQ (noisy intermediate scale quantum) devices that are available today. More importantly, as explained next, errors can arise either due to calibration imperfections or due to external noise (environment). Operationally, it is important to distinguish between the

two types of errors. Unfortunately, this task gets more difficult as the circuits get larger.

Although our results are not restricted to quantum computers and simulators it is instructive to have in mind a device such as a quantum processor with multiple interacting qubits. We start by describing several challenges associated with quantum diagnostics. What connects these topics is that we can address them with our method. In the sections that follow, we apply our methods to these problems.

The methods described in this paper are registered as US provisional patent 63/260501

1.1 Source of errors

There are several sources of errors in NISQ devices and the two main ones are:

- Coherent errors: the device is well isolated from the environment, and the evolution is unitary. However, the device is not executing the unitary operation (“the circuit” in quantum computers) it was instructed to run.
- Incoherent error: interaction with some known or unknown environment leads to non-unitary evolution. This can be either non-unital maps such as thermalization (e.g. spontaneous emission) or unital maps such as decoherence or depolarizing channels (in a unital map, the fully mixed state is a fixed point of the map).

Other sources of errors include state preparation errors and readout errors. However, the first is typically very small and the latter can be resolved by detector calibration procedures.

It is of prime importance to distinguish between coherent and incoherent errors. Coherent errors occur because some parameters in the circuits are not optimally calibrated. In principle, coherent errors can always be fixed by another unitary transformation in the Hilbert space of the original circuit. In contrast, incoherent errors, e.g. decoherence, spontaneous emission, and depolarizing channels, cannot be removed by unitary operations on the circuit alone. Resolving coherent errors from incoherent errors can guide developers and experimentalists where to focus their efforts and also validate if their efforts successfully mitigated the error.

1.2 Holistic vs. One-Circuit Diagnostics

Holistic methods such as quantum volume, randomized benchmarking, and cross entropy benchmarking , characterize the device as a whole. Holistic scores aim to assure a certain level of performance for any circuit. This is appealing for quantum computers where various algorithms may be executed on the same machine. In one-circuit diagnostics, the circuit that executes the computation is given and its performance on the existing hardware is evaluated. Although it may seem that the holistic approach is more useful, the one-circuit approach

has its own merits, and in many cases it will be the first choice in quantifying performance.

1. A given hardware may execute some circuits with sufficiently good fidelity while in others the fidelity is quite poor. It could be that although the holistic score is very low (a poor device), a clever choice of qubits and gates (implementation map) may lead to good fidelity. This is especially relevant for the presently available NISQ devices. After making this choice there is no point in recalculating the holistic score of the whole device (it will remain the same). Instead, the fidelity in the specific choice of implementation map should be evaluated directly. Although it is possible to apply holistic methods to evaluate the selected implementation map the obtained score is not holistic anymore and it may consume a lot of resources compared to other methods for evaluating a specific circuit.

2. In the opposite scenario there is a reasonably good holistic score, but for the circuit of interest, the fidelity is poor. This could be due to an unusually large usage of a noisy gate. A one-circuit diagnostic scheme can be significantly better at detecting such problems.

3. In developing the hardware of a quantum computer, there is often a known gate that is susceptible to noise that the developers want to minimize. Using an ensemble of random circuits to achieve the “error per gate” interpretation as in randomized benchmarking, could be a waste of resources in this case. One can argue that it is possible to simply check the expected functionality of the circuit. Yet, even the case of a single CNOT (or multiple CNOTS) could be quite challenging since coherent errors are interwind with incoherent errors. Thus, a deviation from the ideal CNOT map, may not indicate the presence of an incoherent error.

1.3 Locating the error

Diagnostic processes may have various levels of resolutions. The first goal is to know if there is an error. The next goal is to locate the error, and the third is to classify the type of error or ideally provide the relative weights of various noise mechanisms. Presently, the location task is carried out by applying holistic methods to smaller systems (e.g. CNOT’s and single-qubit gates) that compose the larger device. While this method is useful, it has two limitations that one should keep in mind: i) there could be crosstalk effects that are difficult to detect when checking a circuits element by element; ii) in a given circuit and a given initial condition, it could be that a small level of noise in a good gate is more harmful than other high-noise gates. One trivial reason could be that this gate is used more time than the other gates. Thus there is a motivation to locate the error within the one-circuit diagnostics framework. That is, to run the full circuit (with many qubits) and mark the hotspots that lead to performance degradation. Our approach offers a way to locate the noise within a big circuit without resorting to subsystem benchmarking.

1.4 Measuring purity

Purity, entropy, or the Rényi entropy are Schur concave functions that can be used to quantify the amount of randomness (or lack of it) in quantum or classical systems. The change in the von Neumann entropy, for example, has a major role in quantum thermodynamics and quantum information. Purity and Rényi entropy have a variety of applications in quantum information theory as well. Unfortunately, despite the many insights that these quantities provide, they are not experimentally friendly. They are nonlinear in the density matrix, and therefore cannot be directly associated with observables. Rather, the density matrix should be mapped by measuring a non-scalable number of observables. The basis in which the density matrix is diagonal, is a priori unknown, and therefore all elements in the density matrix have to be evaluated (state tomography).

Several techniques and methods have been suggested to reduce the resources needed for evaluating the purity. In [1] two copies of the system and a control swap interaction are used for evaluating the purity. In [2], single-qubit rotations were used to reduce the number of measurements needed for purity measurement. Reset and reuse of qubits were used in [3] to reduce the resources of purity and higher-order Rényi entropies measurements. Finally, matrix product state methods that assume local buildup of correlation have been studied in [4].

Our approach is based on a single observable that is measured at multiple time points. Thus, the number of observable reduces to one that is evaluated for each number of cycles. That is, the number of measurements is equal to the number of cycles which typically ranges in our methods between three to five. To avoid overhyping, we stress already at this point, that our method detects purity changes and not purity. Furthermore, it is valid only when the change in purity (the dissipation) is small.

1.5 Measuring Entanglement

In the previous section, purity was discussed as an indicator of environment-induced noise. However, purity can be also used for quantifying entanglement buildup between two parts of an isolated system. Entanglement is considered to be the quantum agent responsible for quantum speedups. Nevertheless, it is quite challenging to measure it, especially if no prior information on the circuit exists (a “black box”). If, however, there is an efficient way of evaluating the local purity of a subsystem, it can be used to quantify the entanglement of the subsystem to the other parts of the system. For pure states, a necessary and sufficient condition for the presence of entanglement is that the purity of a subsystem is lower than the purity of the total system (which is one for pure states) [5]. Although our results on measuring purity changes cannot be applied to entanglement measurement as is, we suggest a modification of the experimental protocol that makes our methods applicable to entanglement measurements as well.

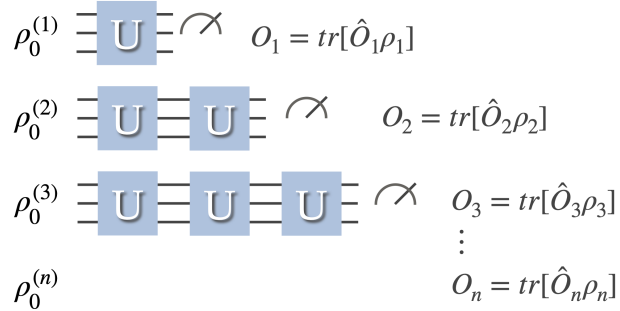


Figure 1: Our methods are based on a set of experiments with a successively increasing number of repetitions of the basic quantum circuit (denote by U). The measured quantities at the end of each experiment are combined to form measures that quantify various dissipation aspects of the system, for example, the total purity change in the circuit and local dissipation in the qubits.

2 Our method

Our method is based on running the circuit of interest multiple times sequentially, measuring a quantity in each run, and adding the various results with proper amplitudes. The most general case is illustrated in Fig. 1. The run we denote by ' k ' is characterized by having k cycles between the initial state preparation and the measurement. In the general case, each run may have a different initial condition $\rho_0^{(k)}$ and a different measurement operator \hat{O}_k (or a POVM). The expectation value O_k is calculated at the end of each run:

$$O_k = \langle \hat{O}_k \rangle = \text{tr}[\rho_k \hat{O}_k]. \quad (1)$$

For clarity, in each run the circuit is measured many times (“shots”) to gain sufficiently low O_k variance. Next, we compute the following sum:

$$A_n^O = \sum_{k=0}^n a_k^{(n)} O_k, \quad (2)$$

and from this sum, we intend to distill information about the purity change and the hotspots of dissipation. Potentially, in the most general case, A_n^O can be a nonlinear function of $\{O_k\}_{k=0}^n$.

2.1 The weak action limit of the \mathcal{S}_n sums

For measuring the change in purity we set $\rho_0^{(k)} = \rho_0$ where ρ_0 can be either a pure state or a mixed state. For the measurement, we set $\hat{O}_k = \rho_0$ which lead to the set observables

$$R_k = \text{tr}[\rho_0 \rho_k], \quad (3)$$

that we refer to as the survival probability (not to be confused with the calligraphic \mathcal{R} used later on for Rényi entropy). For a pure state R_k is the probability to find the system in its initial state. For mixed states it has the same meaning: writing $\rho_0 = \sum_{i=0} p_i |i\rangle \langle i|$, R_k is the probability that the system starts at $|0\rangle$ and found to be in $|0\rangle$ at the end, plus the probability of starting at $|1\rangle$ and ending in $|1\rangle$ and so on. That is, the probability that a system returns to its initial state without any importance to what state it was initially in.

We define the coefficients

$$w_k^{(n)} = \frac{2(2n-1)}{n} \frac{n!^2}{(n-k)!(n+k)!} (-1)^k, \quad (4)$$

$$w_0^{(n)} = 2 - \frac{1}{n}, \quad (5)$$

and denote the resulting $A_n^{\rho_0}$ by \mathcal{S}_n

$$\mathcal{S}_n = \sum_{k=0}^n w_k^{(n)} R_k, \quad (6)$$

where \mathcal{S}_1 is often too trivial to be of use. The first few entries are:

$$\mathcal{S}_2 = \frac{3}{2}R_0 - 2R_1 + \frac{1}{2}R_2, \quad (7)$$

$$\mathcal{S}_3 = +\frac{5}{3}R_0 - \frac{5}{2}R_1 + R_2 - \frac{1}{6}R_3, \quad (8)$$

$$\mathcal{S}_4 = \frac{7}{4}R_0 - \frac{14}{5}R_1 + \frac{7}{5}R_2 - \frac{2}{5}R_3 + \frac{1}{20}R_4. \quad (9)$$

To understand the physical meaning of these series we move from Hilbert space to Liouville space. In Liouville space, the density matrix $\rho_{N \times N}$ is flattened into a column “density vector” of length N^2 i.e. $\rho_{N \times N} \rightarrow |\rho\rangle_{N^2 \times 1}$. As a result the Liouville von Neumann equation of motion $id_t \rho = [H, \rho]$ becomes:

$$id_t |\rho\rangle = H_L |\rho\rangle \quad (10)$$

$$H_L = H \otimes I_N - I_N \otimes H^t \quad (11)$$

where I_N is the identity operator in the original Hilbert space ($N \times N$) and the subscript L indicates that H_L is in Liouville space. For unitary dynamics H_L is hermitian and the resulting evolution operator in Liouville space is unitary: $|\rho_t\rangle = U_{L,t} |\rho_0\rangle$ and $U_{L,t} U_{L,t}^\dagger = I_{N^2}$. If the dynamics is (quantum) Markovian, the Schrödinger-like form (10) still holds but now the generator of motion $X = -iH_L + L$ does not have the form (11). In It is easy to obtain L from the Lindblad equation in Hilbert space (see Sec. 3.1) but we will not need it explicitly here. Due to the Schrödinger-like form, one can write the one cycle evolution operator $|\rho_{k+1}\rangle = U_L |\rho_k\rangle$ as

$$U_L = e^{-i\mathcal{H}_{L,eff}}, \quad (12)$$

where $\mathcal{H}_{L,eff}$ is an effective time-independent Hamiltonian that same evolution as the time-dependent Hamiltonian. Furthermore, the calligraphic font indicates

that we are using for convenience dimensionless operators that already contain the time duration of the cycle. In the more general quantum Markovian case we can write

$$K_L = e^{-i\mathcal{H}_{L,eff} + \mathcal{L}_{eff}} \doteq e^x. \quad (13)$$

Later on, we shall refer to the operator norm of $\|x\|_{op}$ as the action of the circuit. Next, we shall employ the fact that the standard scalar product of matrices in Hilbert space $tr[A^\dagger B]$ reads $\langle A | B \rangle$ in Liouville space where $\langle \cdot | = |\cdot \rangle^\dagger$ as in Hilbert space. Consequently, expectation value can be written as

$$\langle O \rangle = tr[O\rho] = \langle O | \rho \rangle. \quad (14)$$

Combining this with (13) we get $R_k = \langle \rho_0 | e^{kx} | \rho_0 \rangle$. As a result we obtain

$$\mathcal{S}_n = \sum_{k=0}^n w_k^{(n)} \langle \rho_0 | e^{kx} | \rho_0 \rangle = \left\langle \rho_0 \left| \sum_{k=0}^n w_k^{(n)} e^{kx} \right| \rho_0 \right\rangle. \quad (15)$$

This form shows that that \mathcal{S}_n can be seen as an expectation value of the operator $G_n = \sum_{k=0}^n w_k^{(n)} e^{kx}$. Expressions similar to \mathcal{S}_n have been suggested by the current author in [6]. Yet, these expressions were used only for constructing inequalities, and their values were not related to any physical quantities of interest as done here in the weak action regime.

Next, we carry out a Markovian open quantum system analysis in the regime of weak action. We start with an expansion for small x :

$$\mathcal{S}_2 = \left\langle -x + \frac{1}{3}x^3 + \frac{1}{4}x^4 + \frac{7}{60}x^5 + \frac{1}{24}x^6 + \frac{31}{2520}x^7 + \frac{1}{320}x^8 + O(x^9) \right\rangle, \quad (16)$$

$$\mathcal{S}_3 = \left\langle -x + \frac{1}{6}x^3 - \frac{11}{120}x^5 - \frac{1}{12}x^6 - \frac{239}{5040}x^7 - \frac{1}{48}x^8 + O(x^9) \right\rangle, \quad (17)$$

$$\mathcal{S}_4 = \left\langle -x + \frac{2}{15}x^3 - \frac{1}{30}x^5 + \frac{151}{6300}x^7 + \frac{1}{40}x^8 + O(x^9) \right\rangle. \quad (18)$$

Our first key observation is that due to the following property of Hamiltonians in Liouville space

$$\langle \rho | \mathcal{H}_L^{2n+1} | \rho \rangle = 0, \quad (19)$$

all odd terms in \mathcal{S}_n drop out when $\mathcal{L} = 0$. The proof of (19) is given in the Appendix. Thus, when the evolution is unitary

$$\mathcal{S}_2 = \frac{1}{4} \langle x^4 \rangle + O(x^6), \quad (20)$$

$$\mathcal{S}_3 = -\frac{1}{12} \langle x^6 \rangle + O(x^8), \quad (21)$$

$$\mathcal{S}_4 = \frac{1}{40} \langle x^8 \rangle + O(x^9). \quad (22)$$

Consequently, if x is small the \mathcal{S}_n rapidly converges to zero as the number of cycles increases. On the other hand if $x = -i\mathcal{H}_{L,eff} + \mathcal{L}_{eff}$ we obtain

$$\mathcal{S}_2 = -\langle \mathcal{L}_{eff} \rangle + \frac{1}{3} \langle x^3 \rangle + O(x^4), \quad (23)$$

$$\mathcal{S}_3 = -\langle \mathcal{L}_{eff} \rangle + \frac{1}{6} \langle x^3 \rangle + O(x^5), \quad (24)$$

$$\mathcal{S}_4 = -\langle \mathcal{L}_{eff} \rangle + \frac{2}{15} \langle x^3 \rangle + O(x^5). \quad (25)$$

Note, that this time $\langle x^3 \rangle \neq 0$ since it contains term like H^2L and L^3 . Nevertheless, we will assume that in the weak action regime, x^3 has a negligible contribution to \mathcal{S}_2 . Furthermore, by taking $2\mathcal{S}_3 - \mathcal{S}_2$ we get

$$2\mathcal{S}_3 - \mathcal{S}_2 = -\langle \mathcal{L}_{eff} \rangle + O(x^4). \quad (26)$$

By increasing the cycle number it is possible to eliminate higher-order corrections and make the evaluation $\langle \mathcal{L}_{eff} \rangle$ applicable to circuits with larger action. This, however, cannot be done indefinitely, since the measurement uncertainty tends to increase when adding more cycles to eliminate higher-order corrections. In the rest of the paper, for brevity, we drop the “eff” and “L” subscripts from the generators of motion.

3 Applications

3.1 Measuring the matrix element of the dissipator

Equations (23)-(25) show that the \mathcal{S}_n 's provide a direct information on the “dissipator matrix element” in Liouville space. This allows to learn about the active noise mechanisms in a given circuit and also use this information to predict how they affect other circuits. As a first example let us look at a single spin spontaneous emission. The annihilation operator in Hilbert space is $a = \begin{pmatrix} 0 & 0 \\ 1 & 0 \end{pmatrix}$ and the corresponding Liouvillian is:

$$L_{spont} = \xi[a \otimes (a^\dagger)^t - \frac{1}{2}a^\dagger a \otimes I_2 - \frac{1}{2}I_2 \otimes a^\dagger a], \quad (27)$$

where ξ corresponds to the decay rate (the decay time “ T_1 ” is equal to $1/\xi$). Using $|\uparrow_L\rangle = \{1, 0, 0, 0\}$, $|\downarrow_L\rangle = \{0, 0, 0, 1\}$ and $|+_L\rangle = \frac{1}{2}\{1, 1, 1, 1\}$ to denote up, down and plus states in Liouville space, we find that

$$\langle \uparrow_L | L_{spont} | \uparrow_L \rangle = -\xi, \quad (28)$$

$$\langle \downarrow_L | L_{spont} | \downarrow_L \rangle = 0, \quad (29)$$

$$\langle +_L | L_{spont} | +_L \rangle = -\frac{1}{4}\xi. \quad (30)$$

A depolarizing channel can be written as $L_{depol} = L_{spon} + L_{spon}(a \leftrightarrow a^\dagger)$ and it satisfies:

$$\langle \uparrow_L | L_{depol} | \uparrow_L \rangle = -\xi, \quad (31)$$

$$\langle \downarrow_L | L_{depol} | \downarrow_L \rangle = -\xi, \quad (32)$$

$$\langle +_L | L_{depol} | +_L \rangle = -\frac{1}{2}\xi. \quad (33)$$

For a pure decoherence channel the Lindblad operator is the Pauli σ_z and the resulting Liouvillian is:

$$L_{decoh} = \frac{1}{2}\xi[\sigma_z \otimes \sigma_z - I_2 \otimes I_2], \quad (34)$$

and we get

$$\langle \uparrow_L | L_{decoh} | \uparrow_L \rangle = 0, \quad (35)$$

$$\langle \downarrow_L | L_{spon} | \downarrow_L \rangle = 0, \quad (36)$$

$$\langle +_L | L_{spon} | +_L \rangle = -\frac{1}{2}\xi. \quad (37)$$

Thus by evaluating $-\mathcal{S}_2$ (or $\mathcal{S}_{n>2}$) for the initial states $|\downarrow\rangle$ $\langle\downarrow|$, $|\uparrow\rangle$ $\langle\uparrow|$ and $|+\rangle$ $\langle+|$ it is possible to identify the decay mechanism of the spin. If the channel is thermal, one can use the ratio $\langle \uparrow_L | L_\beta | \uparrow_L \rangle / \langle \downarrow_L | L_\beta | \downarrow_L \rangle = e^{-\beta\omega}$ for evaluating the inverse temperature β given the energy gap of the qubit ω . We conclude that by using different initial condition it is possible to investigate the nature of some unknown environment.

The reader may be puzzled at this point since the decoherence time, for example, could be simply evaluated by measuring $\sqrt{\langle \sigma_x \rangle^2 + \langle \sigma_y \rangle^2}$ as a function of time in the absence of driving. Yet, our method enables to extract information on the dissipator under arbitrary weak driving which fits the spirit of “one-circuit diagnostics” rather than using a dedicated circuit for the job.

In the presence of multiple qubits evaluation of \mathcal{S}_2 for the initial state $|+\rangle \otimes |+\rangle \otimes |+\rangle \dots$ will yield the sum of the local decoherence rates which represent the leading term in the purity loss in the total circuit as explained in the next section. Interestingly, even when running the whole circuit it is possible to evaluate the individual qubit dissipation rate using the methods we present in Sec. 3.4 and in Fig. 4.

3.2 Measuring small purity changes using \mathcal{S}_n

Let us look at the change in purity after one cycle in the weak action regime:

$$\begin{aligned}
\Delta \text{tr} \rho^2 &= \langle 0 | e^{x^\dagger} e^x | 0 \rangle - \langle 0 | 0 \rangle \\
&= \langle 0 | (1 + x^\dagger + x^{\dagger 2}/2)(1 + x + x^2/2) | 0 \rangle - \langle 0 | 0 \rangle + O(x^3, x^2 x^\dagger, \dots) \\
&= \langle x + x^\dagger + x^{\dagger 2}/2 + x^2/2 + x^\dagger x \rangle + O(x^3, x^2 x^\dagger, \dots) \\
&= \langle 2\mathcal{L} - i\{\mathcal{H}, \mathcal{L}^\dagger\} + i\{\mathcal{H}, \mathcal{L}\} + \mathcal{L}^{\dagger 2}/2 + \mathcal{L}^2/2 + \mathcal{L}^\dagger \mathcal{L} \rangle + O(x^3, x^2 x^\dagger, \dots).
\end{aligned} \tag{38}$$

Thus when \mathcal{L} and \mathcal{H} are small the second-order terms are negligible and we get

$$\Delta \text{tr} \rho^2 = -2\mathcal{S}_n + O(\mathcal{L}^2, \mathcal{L}\mathcal{H}, \mathcal{H}\mathcal{L}). \tag{39}$$

For some dissipators, the expression (38) simplifies and further approximations can be made. For example, for depolarizing channel and for all Hermitian Lindblad operators, e.g., decoherence operators, it holds that $\mathcal{L} = \mathcal{L}^\dagger$ and therefore:

$$\Delta \text{tr} \rho^2 = 2\langle \mathcal{L} \rangle + 2\langle \mathcal{L}^\dagger \mathcal{L} \rangle + O(x^3, x^2 x^\dagger, \dots). \tag{40}$$

Since $\langle \mathcal{L}^\dagger \mathcal{L} \rangle \geq \langle \mathcal{L} \rangle^2$ it follows that $\Delta \text{tr} \rho^2 \geq \langle \mathcal{L} \rangle + 2\langle \mathcal{L} \rangle^2$. For pure state $\langle \mathcal{L} \rangle \leq 0$ so $2\langle \mathcal{L} \rangle$ slightly overestimates the rate and the term $2\langle \mathcal{L} \rangle^2$ reduces this overestimation. Hence we can write

$$\Delta \text{tr} \rho^2 \simeq 2\langle \mathcal{L} \rangle + 2\langle \mathcal{L} \rangle^2 = -2\mathcal{S}_2 + 2\mathcal{S}_2^2. \tag{41}$$

Figure 2 test our purity change estimation on random circuits. Each point on the horizontal axis corresponds to a different circuit. A randomly chosen (weak) Hamiltonian generates the unitary drive and each qubit undergoes decoherence at a different random rate (the rate change from one circuit to another but not during the evolution). The Blue circles correspond to the exact value of the purity change in one cycle $\text{tr} \rho_1^2 - \text{tr} \rho_0^2$, and the red squares correspond to our $-2\mathcal{S}_2$ estimation. Since the Lindblad operator is hermitian (decoherence) we also plot in green diamonds the refinement (41) which substantially improves the purity estimation accuracy for higher purity changes.

3.3 Measuring entanglement

In continuation to Sec. (1.5), one of the entanglement measures for a pure state ρ_{AB} in a bipartite system AB is directly related to the purity, or more accurately to the Rényi entanglement entropy of order two [5]:

$$\mathcal{R}_2 = -\ln \text{tr}[\rho_A^2], \tag{42}$$

where $\rho_A = \text{tr}_B \rho_{AB}$. Thus, methods for evaluating the purity of a subsystem can be exploited to quantify entanglement as well. While in some methods for

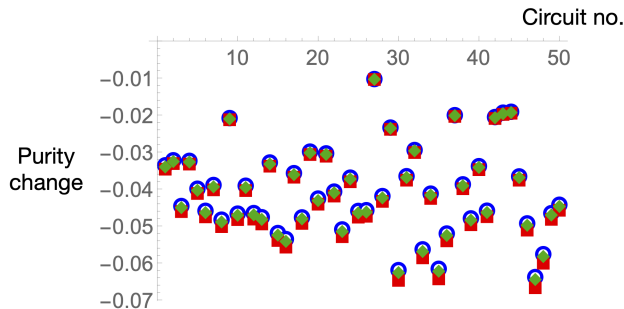


Figure 2: Estimating the purity change in a four-qubit weak action random circuits with random decoherence in each qubit. (b) Each point on the horizontal axis corresponds to a different circuit and different decoherence rates. The blue circles mark the exact purity change, the red square corresponds to our $-2\mathcal{S}_2$ method, and green diamonds stand for the refinement $-2\mathcal{S}_2 + 2\mathcal{S}_2^2$, in Eq. (41).

evaluating the purity, the application to entanglement measurement is straightforward, here there is an interesting difference that requires a modification in the \mathcal{S}_n experimental protocol.

The \mathcal{S}_n method for evaluating the purity change in the first cycle (Sec. 3.2) assumes that the dynamics is periodic and Markovian, or alternatively stated, a periodic CP map. However, if the AB system evolves unitarily, the reduced dynamics of ρ_A is typically non-markovian and therefore \mathcal{S}_n will not yield information on the purity change in A. To induce a periodic CP map we use the following recipe. Assume the initial state is a product pure product state

$$\rho_0 = |\psi_A\rangle\langle\psi_A| \otimes |\psi_B\rangle\langle\psi_B|. \quad (43)$$

After applying one cycle of the unitary evolution we reset subsystem B to its initial state and only then perform the unitary evolution of the next cycle. In the general case, the same is carried out for the other cycles so that:

$$\rho_n = \rho_{n,A} \otimes |\psi_B\rangle\langle\psi_B|, \quad (44)$$

$$\rho_{n+1} = U(\rho_{n,A} \otimes |\psi_B\rangle\langle\psi_B|)U^\dagger. \quad (45)$$

The resetting generate a periodic CP map for which we can apply our method. The resetting changes evolution, however for the first cycle $\rho_{A,1}^{\text{no reset}} = \rho_{A,1}^{\text{reset}}$. Thus, by evaluating the purity change in the first cycle of the system with the reset, we obtain the purity change in the original system. Starting in a pure state we finally get

$$\Delta\mathcal{R}_2 = \mathcal{R}_2^{\text{fin}} = -\ln \text{tr} \rho_{\text{fin},A}^2 = -\ln(1 + \Delta \text{tr} \rho_A^2) \simeq \mathcal{S}_{n,A}^{\text{reset}}, \quad (46)$$

where $\mathcal{S}_{n,A}^{\text{reset}}$ stands for the purity change evaluation in subsystem A with the reset protocol. In Fig. 3 we took a six-qubit system and partitioned it into

Figure 3: (a) A numerical simulation of measuring the entanglement in a six-qubit system using our periodic reset protocol (b). The blue circles represent the exact value of the Rényi 2 entanglement entropy between two sets of three qubits. The red squares correspond to our S_2^{reset} method. Each point on the horizontal axis corresponds to a different small action random circuit. As expected, the method works well when the entanglement is small (roughly 0.07 in this case).

two parts with three qubits each. Random Hamiltonians in the space of the six qubits were used to weakly entangle the two parts. To make sure the dynamics is in the weak action regime the operator norm of the Hamiltonians was restricted to values below 0.8. The blue circles in Fig. 3 show the exact calculation S_2 , and the red square corresponds to our reset method (46). Fig. 3b illustrates the two-cycle run in the reset protocol.

3.4 Dissipation hot spots - locating the incoherent errors in the circuit

In trying to apply our method to other quantities (observables) it's useful to point the key elements in the S_n method:

1. The choice of $w_k^{(n)}$ lead to the cancellation of some of the leading even-order terms in the weak action regime.
2. The odd terms are zero when $\mathbf{x} = i\mathbf{H}$, $\text{tr}(\mathbf{H}^{2k+1}) = 0$.
3. For periodic CP maps, the first-order term is not zero, but it depends only

on the dissipative part of the dynamics. Thus the first-order term can be used to study the interaction of the system with the environment.

Property #1 makes no use of the fact that the quantity of interest is purity. Property #2 was proved in the first part of the Appendix for survival probabilities. That is, the observable A was equal to the initial density matrix ρ_0 . As it turn out, for a general observable $A = A^\dagger$ in Hilbert space, $\langle A | \mathcal{H}_L^{2n+1} | \rho_0 \rangle \neq 0$. Yet, we show in the second part of the appendix that for observables satisfying $[A, \rho_0] = 0$ it holds that

$$\langle A | \mathcal{H}_L | \rho_0 \rangle = 0. \quad (47)$$

Next, we set $\hat{O}_k = A$ in (2) and for the coefficients we choose $a_k^{(n)} = w_k^{(n)}$ as before, and we get

$$\mathcal{S}_n^A = \sum_{k=0}^n w_k^{(n)} A_k = \sum_{k=0}^n w_k^{(n)} \text{tr}[A \rho_k], \quad (48)$$

that, as before, we can write as

$$\mathcal{S}_n^A = \sum_{k=0}^n a_k^{(n)} \langle A | e^{kx} | \rho_0 \rangle = \left\langle A \left| \sum_{k=0}^n a_k^{(n)} e^{kx} \right| \rho_0 \right\rangle. \quad (49)$$

Using (47) we obtain

$$\mathcal{S}_2^A = -\langle A | \mathcal{L} | \rho_0 \rangle + O(x^3), \quad (50)$$

$$2\mathcal{S}_3^A - \mathcal{S}_2^A = -\langle A | \mathcal{L} | \rho_0 \rangle + O(x^4). \quad (51)$$

Note, that here the third order does not cancel out. Yet, by running one more cycle and using (51) the third order can be eliminated for (for unitary and nonunitary evolution both). To understand what this quantity means we evaluate the ‘‘dissipative change’’ in $\langle A \rangle$:

$$\begin{aligned} \Delta_{\text{diss}} \langle A \rangle &= \Delta \langle A \rangle - \Delta_{\text{no diss}} \langle A \rangle \\ &= \langle A | e^x | \rho_0 \rangle - \langle A | \rho_0 \rangle - (\langle A | e^{-i\mathcal{H}} | \rho_0 \rangle - \langle A | \rho_0 \rangle) \\ &= \langle A | (1 + x + x^2/2) | \rho_0 \rangle - \langle A | (1 - i\mathcal{H} - \mathcal{H}^2/2) | \rho_0 \rangle + O(x^3, x^2 x^\dagger, \dots) \\ &= \langle A | \mathcal{L} + (i\mathcal{H} + \mathcal{L})^2/2 + \mathcal{H}^2/2 | \rho_0 \rangle + O(x^3, x^2 x^\dagger, \dots) \\ &= \langle A | \mathcal{L} + \mathcal{L}^2/2 + i\{\mathcal{L}, \mathcal{H}\}/2 | \rho_0 \rangle + O(x^3, x^2 x^\dagger, \dots). \end{aligned} \quad (52)$$

If the Lindblad operators that generates \mathcal{L} are hermitian and the dissipator is incoherent i.e. $\langle \text{coherences} | \mathcal{L} | \text{diagonal state} \rangle = 0$ (the map does not create coherences when starting in a diagonal state) then $\langle A | \{\mathcal{L}, \mathcal{H}\} | \rho_0 \rangle = 0$. Another option for eliminating the $\mathcal{H}\mathcal{L}$ term is to run another circuit with $\mathcal{H} \rightarrow -\mathcal{H}$,

and measure the mean $\frac{1}{2}[\mathcal{S}_2^A(\mathcal{H}) + \mathcal{S}_2^A(-\mathcal{H})]$. Assuming that $\{\mathcal{L}, \mathcal{H}\}$ is either zero or removed we get:

$$\Delta_{diss} \langle A \rangle = -\mathcal{S}_2^A + O(\mathcal{L}^2) + O(x^3), \quad (53)$$

$$\Delta_{diss} \langle A \rangle = -2\mathcal{S}_3^A + \mathcal{S}_2^A + O(\mathcal{L}^2) + O(x^4), \quad (54)$$

$$\Delta_{diss} \langle A \rangle = -5\mathcal{S}_4^A + 4\mathcal{S}_3^A + O(\mathcal{L}^2) + O(x^5). \quad (55)$$

Note that the driving term can be significant so the cancellation of the third order can be important.

To illustrate our finding, in Fig. 4, we consider a four-qubit example with a random weak unitary driving. Qubits 2 and 4 are noisy (inset). The driving Hamiltonian is chosen with random elements in the interval $\{\pm 0.1 \pm 0.1i\}$ and the time interval is $T = 1$ which leads to an average action of $[\max(H) - \min(H)]T = 0.08$. The initial state is $|++++\rangle$. The decoherence rate of qubit #2 is $\xi_2 = 1e - 3$ ($\tau_{(2)} = 1000$) and in qubit #4 it is $\xi_4 = 7e - 4$ ($\tau_{(4)} = 1428.6$). Without driving the coherence $\langle \sigma_x \rangle$ of qubit 2 decays from 1 to 0.9995. Qubits 1 and 3 are not directly dissipated, they only interact with dissipative qubits. The observables of interest are the $\langle \sigma^x \rangle$ of each qubit. Before studying the dissipative change in $\langle \sigma^x \rangle$ of each qubit we plot in Fig. 4a the “total” change (driving + dissipation) in qubit i , $\Delta \langle \sigma_i^x \rangle = \text{tr}[(\rho_1 - \rho_0)\sigma_i^x]$. The dissipative qubits 2 & 4 seem no different from the non-dissipative qubits 1 & 3. Yet, by running three [Fig. 4(b)] or four [Fig. 4(c)] cycles, we can employ our methods and correctly evaluate the decoherence rate of the different qubits despite the random unitary in the background.

Finally, let us point out that the “hotspot” may not be individual qubits but gates. If the gate mechanism itself involves some interaction with the environment, then only when this gate is activated noise will appear in the system. The qubits that are affected by this gate will appear as noisy.

4 Relieving the weak action restriction

Due to the weak action validity regime, it is not possible to immediately apply the methods here presented to any quantum circuit. Yet there are two alternatives that enable indirectly to address any circuit provide the noise is sufficiently small.

4.1 “Weakened circuits”

The first option is to have a “weak version” of the original circuit. This can be done by simply making all the RF/laser control weaker by a factor $\gamma < 1$. Assuming the dissipation in the original circuit is weak the new evolution operator is $e^{-i\gamma\mathcal{H}_L^{eff} + \mathcal{L}^{eff}}$ will be in the weak action regime and our methods can be applied. Although we presently do not know how to analytically connect

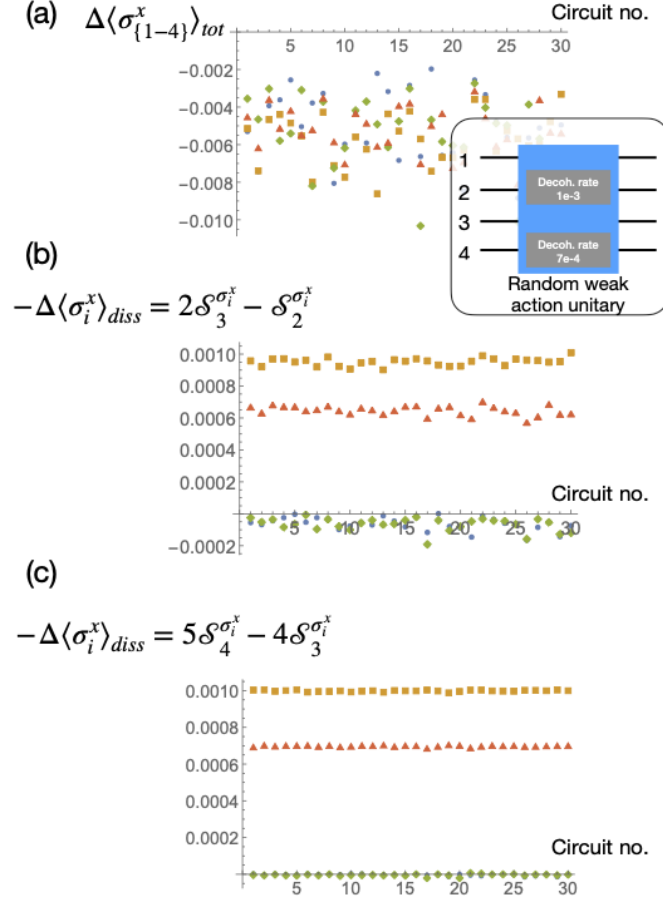


Figure 4: In this example, four qubits interact via a random Hamiltonian (inset). Qubit #2 undergoes decoherence at a rate $\xi_2 = 0.001$ and the decoherence rate of qubit #4 is $\xi_4 = 0.0007$. Qubit #1 and #3 are not directly dissipated. In all plots, the x axis corresponds to different random Hamiltonians. Figure (a) shows that the change in the σ^x expectation values of the qubits is roughly the same for all qubits. Thus it is not possible to tell which qubits are losing coherence. However, when using our method [Fig. (b) & (c)] to evaluate the dissipative contribution to the change in $\langle\sigma_i^x\rangle$, it becomes clear that qubit #2 (orange squares) and qubit #4 (red triangles) have clear dissipative change while qubit #1 (blue circles) and qubit #3 (green diamonds) experience no dissipative change. In Fig. (b) three cycles are used, which lead to fourth-order correction in the action (54). As a result, the dissipative change of qubits 1# and 3# is not exactly zero. In (c) we use 4 cycles, and consequently, the correction is of order five in the action (55). Here it is clear that our method correctly retrieves the values of the decoherence rate ξ_2, ξ_4 and the null rates of qubits 1 and 3.

the change in purity in the weakened circuit to the purity change in the original large action circuit, one can argue that the weak action version has the same implementation map and it is susceptible to the same noise mechanism as the original circuit. In particular, if non-negligible dissipation effects appear already at the weakened version they are unlikely to just fade away in the original circuit. Thus it could be a good practice to first use the weakened version to optimize the performance of the device and only then proceed to check the original circuit.

Another way of using the weakened circuit is to moderately increase the action of the weakened circuit but use more cycles to evaluate higher-order \mathcal{S}_n 's [and combinations of \mathcal{S}_n 's as in (55)]. Interestingly, when using sufficiently weak local dissipators on each qubit, we find that the purity loss is roughly independent of the strength of the drive (the action of the noiseless circuit) even if it is very strong. We observed this behavior when the purity loss was ~ 0.03 or less. If this finding is general, it paves the way to using weakened circuits for quantifying the noise in arbitrary circuits that are subjected only to local decay and decoherence.

4.2 Using the inverse circuit

Another alternative is to implement the circuit and immediately after implementing the inverse circuit. Since the dissipation mechanisms are the same for the inverse circuit, it follows that if the evolution operator (with the dissipation) in Liouville space is given by $K = e^{-i\mathcal{H}+\mathcal{L}}$, then the evolution operator of the inverse circuit is given $K_I = e^{-i\mathcal{H}_I+\mathcal{L}}$ where $\mathcal{H}_I = -\mathcal{H}+d\mathcal{H}$ where $d\mathcal{H}$ represent potential coherent errors. For simplicity we Next we compare the purity in one cycle:

$$\Delta tr[\rho^2]_K = \langle r_0 | K^\dagger K | r_0 \rangle - \langle r_0 | r_0 \rangle \quad (56)$$

to the purity create by the circuit and its noisy inverse

$$\Delta tr[\rho^2]_{K_I K} = \langle r_0 | (K_I K)^\dagger K_I K | r_0 \rangle - \langle r_0 | r_0 \rangle \quad (57)$$

Treating L as small and using the derivative of the exponential map we get:

$$K = e^{-i\mathcal{H}+\mathcal{L}} = e^{-i\mathcal{H}} \left\{ 1 + \sum_{k=0}^{\infty} \frac{1}{k+1} [(+i\mathcal{H})^{(k)}, \mathcal{L}] \right\} + O(\mathcal{L}^2) \quad (58)$$

where $[A^{(1)}, B] = [A, B]$, $[A^{(2)}, B] = [A, [A, B]]$, $[A^{(3)}, B] = [A, [A, [A, B]]]$ and so on. After some algebra we show in Appendix II that:

$$\Delta tr[\rho^2]_K = \left\langle r_0 \left| 1 + \sum_{k=0}^{\infty} \frac{2}{k+1} [(+i\mathcal{H})^{(k)}, \mathcal{L}] \right| r_0 \right\rangle + O(\mathcal{L}^2) \quad (59)$$

which is an extension of eq. (38) to large \mathcal{H} . Next, we calculate the change in purity of the inverse circuit. In Appendix II we get:

$$K_I K = 1 + \sum_{k=0}^{\infty} \frac{2}{k+1} [(+i\mathcal{H})^{(k)}, \mathcal{L}] + O(\mathcal{L}^2) \quad (60)$$

and finally the purity

$$(K_I K)^\dagger K_I K = 1 + \sum_{k=0}^{\infty} \frac{2}{k+1} \{ [(-i\mathcal{H})^{(k)}, \mathcal{L}] + [(-i\mathcal{H})^{(k)}, \mathcal{L}]^\dagger \} + O(\mathcal{L}^2) \quad (61)$$

this is a positive operator so for a state ϕ it holds that $\langle \phi | [(-i\mathcal{H})^{(k)}, \mathcal{L}]^\dagger | \phi \rangle = \langle \phi | [(-i\mathcal{H})^{(k)}, \mathcal{L}] | \phi \rangle$ as a result we get that:

$$\langle r_0 | (K_I K)^\dagger K_I K | r_0 \rangle = 1 + \sum_{k=0}^{\infty} \frac{4}{k+1} [(-i\mathcal{H})^{(k)}, \mathcal{L}] \quad (62)$$

and we get

$$\begin{aligned} \Delta tr[\rho^2]_{K_I K} &= \left\langle r_0 \left| \sum_{k=0}^{\infty} \frac{4}{k+1} [(-i\mathcal{H})^{(k)}, \mathcal{L}] \right| r_0 \right\rangle + O(\mathcal{L}^2) \\ &= 2 \left\langle r_0 \left| \sum_{k=0}^{\infty} \frac{2}{k+1} [(-i\mathcal{H})^{(k)}, \mathcal{L}] \right| r_0 \right\rangle + O(\mathcal{L}^2) \\ &= 2\Delta tr[\rho^2]_K + O(\mathcal{L}^2) \end{aligned} \quad (63)$$

δH represents the presence a potential unitary error. We now make the approximation $\Delta tr[\rho^2]_{\delta\mathcal{H} \neq 0} = \Delta tr[\rho^2]_{\delta\mathcal{H} = 0}$ which means that a slight coherent error will not affect the leading orders in the purity loss of the circuit+inverse system. Thus we can replace K'^\dagger with K^\dagger . Next, we study the purity change in the circuit that contains the original circuit and its inverse. To make a point we start with ρ_0 which can be either mixed or pure.

Concluding remarks

In this paper, we derived several tools that are based on collecting data from several different repetitions of the same circuit to retrieve information on the dissipative effects that take place in the quantum device (circuit). It was shown how to measure the purity change and even how to differentiate between different noise mechanisms. Our approach also enables to locate the error in specific parts of the circuit while running the whole circuit. Thus, it saves the need to evaluate each part of the system separately in order to isolate the problem. Since we use only a few observable regardless of the system size, our approach is scalable. Another interesting application that is unrelated to diagnostics, is entanglement measurement in isolated systems. We demonstrated that by incorporating a reset to part of the system in our basing protocol it is possible to measure the Rényi 2 entanglement. While these methods can be valuable for developers, they can also be useful for end-users that want to verify the performance of the device just before using it.

Appendix I - Derivation of $\langle \rho_0 | H_L^{2n+1} | \rho_0 \rangle = 0$

Let start with simple case of $n=0$. By definition H it holds that

$$\begin{aligned} \langle \rho_0 | H_L | \rho_0 \rangle &= \langle \rho_0 | [H, \rho_0] \rangle = \text{tr}(\rho_0^\dagger [H, \rho_0]) \\ &= \text{tr}(\rho_0 H \rho_0 - \rho_0 \rho_0 H) = 0 \end{aligned} \quad (64)$$

note that the only needed property of property ρ_0 is hermiticity.

$$\begin{aligned} \langle \rho_0 | H_L^{2n+1} | \rho_0 \rangle &= -(\langle \rho_0 | H_L^n \rangle H_L (H_L^n | \rho_0)) \\ &= \langle r | H_L | r \rangle = \text{tr}(r^\dagger [H, r]) \\ &= \text{tr}(r^\dagger H r - r^\dagger r H) = \text{tr}\{(r r^\dagger - r^\dagger r) H\}. \end{aligned} \quad (65)$$

Thus if $r^\dagger = r$ (in Hilbert space)

$$[H, [H, [H, \rho_0]]]^\dagger = [[[\rho_0, H], H], H] = (-1)^n [H, [H, [H, \rho_0]]]. \quad (66)$$

In the second part of the appendix show that if and observable $A = A^\dagger$ satisfies $[A, \rho_0] = 0$ it holds that

$$\langle A | H_L | \rho_0 \rangle = 0. \quad (67)$$

The derivation is straight forward and similar to (64)

$$\begin{aligned} \langle A | H_L | \rho_0 \rangle &= \langle A^\dagger | [H, \rho_0] \rangle \\ &= \text{tr}(A^\dagger H \rho_0 - A^\dagger \rho_0 H) \\ &= \text{tr}([\rho_0, A^\dagger] H) = 0. \end{aligned} \quad (68)$$

Appendix II - purity change with the inverse circuit

Using the identity

$$[A^{(k)}, B]^\dagger = (-1)^k [(A^\dagger)^{(k)}, B^\dagger] = [(-A^\dagger)^{(k)}, B^\dagger], \quad (69)$$

we get $[(i\mathcal{H})^{(k)}, \mathcal{L}]^\dagger = [(i\mathcal{H})^{(k)}, \mathcal{L}^\dagger]$ so that

$$\begin{aligned} K^\dagger K &= \left\{ 1 + \sum_{k=1}^{\infty} \frac{1}{k+1} [(i\mathcal{H})^{(k)}, \mathcal{L}]^\dagger + O(\mathcal{L}^2) \right\} e^{+i\mathcal{H}} \\ &\times e^{-i\mathcal{H}} \left\{ 1 + \sum_{k=1}^{\infty} \frac{1}{k+1} [(i\mathcal{H})^{(k)}, \mathcal{L}] + O(\mathcal{L}^2) \right\}. \end{aligned} \quad (70)$$

Using the fact $\langle \phi | [(-i\mathcal{H})^{(k)}, \mathcal{L}] | \phi \rangle$ is real it holds that

$$\langle \phi | [(i\mathcal{H})^{(k)}, \mathcal{L}] | \phi \rangle = \langle \phi | [(i\mathcal{H})^{(k)}, \mathcal{L}]^\dagger | \phi \rangle, \quad (71)$$

and keeping only $O(\mathcal{L})$ we get:

$$K^\dagger K = 1 + \left(\sum_{k=1}^{\infty} \frac{2}{k+1} [(i\mathcal{H})^{(k)}, \mathcal{L}] + h.c. \right) + O(\mathcal{L}^2). \quad (72)$$

Dealing with the inverse circuit

To deal with K_I we write it as $K_I = (e^{-i\mathcal{H}+\mathcal{L}^\dagger})^\dagger$

$$e^{-i\mathcal{H}+\mathcal{L}^\dagger} = e^{-i\mathcal{H}} \left\{ 1 + \sum_{k=0}^{\infty} \frac{1}{k+1} [(+i\mathcal{H})^{(k)}, \mathcal{L}^\dagger] \right\} + O(\mathcal{L}^2). \quad (73)$$

Thus

$$\begin{aligned} K_I K &= \left\{ 1 + \sum_{k=1}^{\infty} \frac{1}{k+1} [(+i\mathcal{H})^{(k)}, \mathcal{L}^\dagger] \right\} + O(\mathcal{L}^2) \\ &\times \left\{ 1 + \sum_{k=1}^{\infty} \frac{1}{k+1} [(+i\mathcal{H})^{(k)}, \mathcal{L}] \right\} + O(\mathcal{L}^2) = \end{aligned} \quad (74)$$

$$1 + \sum_{k=1}^{\infty} \frac{2}{k+1} [(+i\mathcal{H})^{(k)}, \mathcal{L}] + O(\mathcal{L}^2). \quad (75)$$

where we have used (69) to get

$$\sum_{k=0}^{\infty} \frac{1}{k+1} [(i\mathcal{H})^{(k)}, \mathcal{L}^\dagger]^\dagger = \sum_{k=0}^{\infty} \frac{1}{k+1} [-[(-i\mathcal{H})^\dagger]^{(k)}, \mathcal{L}]. \quad (76)$$

References

- [1] Norbert M Linke, Sonika Johri, Caroline Figgatt, Kevin A Landsman, Anne Y Matsuura, and Christopher Monroe. Measuring the rényi entropy of a two-site fermi-hubbard model on a trapped ion quantum computer. *Physical Review A*, 98(5):052334, 2018.
- [2] A. Elben, B. Vermersch, C. F. Roos, and P. Zoller. Statistical correlations between locally randomized measurements: A toolbox for probing entanglement in many-body quantum states. *Phys. Rev. A*, 99:052323, May 2019.
- [3] Justin Yirka and Yiğit Subaşı. Qubit-efficient entanglement spectroscopy using qubit resets. *Quantum*, 5:535, 2021.
- [4] BP Lanyon, C Maier, Milan Holzäpfel, Tillmann Baumgratz, C Hempel, P Jurcevic, Ish Dhand, AS Buyskikh, AJ Daley, Marcus Cramer, et al. Efficient tomography of a quantum many-body system. *Nature Physics*, 13:1158, 2017.

- [5] Ryszard Horodecki, Paweł Horodecki, Michał Horodecki, and Karol Horodecki. Quantum entanglement. *Rev. Mod. Phys.*, 81:865–942, Jun 2009.
- [6] Tanmoy Pandit, Alaina M Green, C Huerta Alderete, Norbert M Linke, and Raam Uzdin. Bounds on the survival probability in periodically driven quantum systems. *arXiv preprint arXiv:2105.11685*, 2021.